Fabrication of high surface area ribbon electrodes for use in redox flow batteries via coaxial electrospinning

As Published: 10.1016/j.est.2020.102079

Publisher: Elsevier BV

Persistent URL: https://hdl.handle.net/1721.1/133458

Version: Author's final manuscript: final author's manuscript post peer review, without publisher's formatting or copy editing

Fabrication of high surface area ribbon electrodes for use in redox flow batteries via coaxial electrospinning

Shashi Yadav[1]*, Matt D R Kok[2]*, Antoni Forner-Cuenca[3,4], Kevin M Tenny[4,5,] Yet-Ming Chiang[4,6], Fikile R Brushett[4,5], Rhodri Jervis[2], Paul R Shearing[2], Dan Brett[2], Edward P L Roberts[7], Jeff T Gostick[1†]

[1]Porous Materials Engineering and Analysis Lab, Department of Chemical Engineering, University of Waterloo, 200 University Avenue West, Waterloo, Ontario N2L3G1, CA.

[2]Electrochemical Innovation Lab, Department of Chemical Engineering, University College London, London WC1E 6BT, UK

[3]Membrane Materials and Processes, Department of Chemical Engineering and Chemistry, Eindhoven University of Technology, PO Box 513, 5600 MB Eindhoven, NL.

[4]Joint Center for Energy Storage Research, US, Massachusetts Institute of Technology, Cambridge, Massachusetts 02139, USA

[5]Department of Chemical Engineering, Massachusetts Institute of Technology, 77 Massachusetts Avenue, Cambridge, Massachusetts 02139, USA

[6]Department of Materials Science and Engineering, Massachusetts Institute of Technology, 77 Massachusetts Avenue, Cambridge, Massachusetts 02139, USA

[7]Department of Chemical and Petroleum Engineering, University of Calgary, 2500 University Dr NW, Calgary, Alberta T2N 1N4, CA

*These authors contributed equally to this work

[†]Corresponding Author: jgostick@uwaterloo.ca

Abstract

A method for the preparation of electrospun with fibers possessing a ribbon-like cross-sectional shape was developed. These materials could prove beneficial as flow-through electrodes, since ribbons provide a higher surface-to-volume ratio compared to fibers, thereby providing higher reactive surface area at a given porosity. Fabrication of these materials was accomplished by electrospinning a coaxial fiber with a polystyrene core and polyacrylonitrile shell, followed by leaching of the core material leading to the collapse of the shell into a flat ribbon. The surviving shell was then carbonized to make an electrically conductive and electrochemically reactive fibrous structure. Analysis by x-ray computed tomography showed that ribbons of approximately 400 nm × 800 nm were produced, and experimental characterization revealed that they did indeed offer higher volumetric surface area than previously reported electrospun cylindrical fiber electrodes. The electrodes were characterized for various physical and transport properties and compared to commercial Freudenberg H23 carbon

paper in terms of performance in a vanadium redox flow battery. The ribbon-based electrode had better performance and higher power density than commercial Freudenberg H23 electrode in the activation region, though suffered early onset of mass transfer limitations.

1. Introduction

The increase in energy demand and concern over climate change have shifted focus to using renewable energy resources like wind and solar power. These renewable energy sources, though environmentally friendly, are intermittent and require large-scale energy storage to buffer the temporal mismatch between power generation and consumption. Conventional batteries, such as lead-acid and lithium-ion batteries, are quite mature and find application in automobiles and electronics as well as in large scale energy storage. The electro-active material in these batteries is stored in their electrodes. Thus, to increase their energy capacity, thicker or generally larger electrodes are required [1]. However, increasing thickness also increases the resistance to electron and mass transport, thereby increasing the voltage drop and inefficiency [2]. Thus, in a conventional battery, a trade-off has to be made between high energy density and high efficiency [3], [4]. This problem is resolved in flow batteries because of their decoupled energy and power density feature. Their energy density is not a function of electrode thickness and can be increased by simply increasing the volume of electrolyte stored [5]. Power density, however, can be augmented by increasing the stack size or by improving the cell design [5]. Still, the energy and power density of redox flow batteries (RFBs) are lower than those of conventional batteries [5] and need to be improved to accelerate commercialization.

A common approach to improve the efficiency of the electrode reaction is to adorn the surfaces of the porous electrode with catalytic materials [6]. The present work however focuses entirely on create an improved physical structure, via electrospinning, that has increased surface area for reaction, and improved permeability for flow. Adorning the surfaces of such an electrode with catalytic sites can additionally be attempted to further enhance the performance [7], [8], but this was not explored in the present work. In RFBs the importance of increasing surface area has been demonstrated by simply stacking together multiple layers of carbon paper [9]. This approach, however, increases the overall electrode thickness, consequently increasing the ohmic losses in the cell [10]. In another study, Zhou et al [11] increased the surface area of carbon paper electrode by etching, using a KOH activation method. This treatment caused the formation of nano-pores on the electrode surface resulting in a specific surface area of 42.7 $m^2 \cdot g^{-1}$ [11]. Increasing surface area in this way is not as effective as it may seem, since these pores are only accessed via diffusion processes, making them easily mass transfer limited. Other approaches that have been investigated are coating high surface area materials, such as graphene, carbon black and carbon nanotubes, onto the surface of carbon fibers [12]–[14] using techniques such as dip coating, chemical vapour deposition (CVD), etc. The drawback of using dip coating is that the high surface area material coated on carbon fiber is held together by weak Van der Waal forces, which can be easily broken by the electrolyte flowing through the electrode leading to reduced durability [11]. While CVD covalently binds the high surface area material and the carbon fiber together the technique is both expensive and time consuming [11].

Both approaches mentioned above sought to increase the surface area of commercially available carbon felt or carbon paper electrodes, which have fibers of size d≈10 µm and porosity of ca. 80% [15]. Kok et al [16] utilized multi-physics modelling to determine the optimal electrode properties for achieving high power density in RFB's and suggested electrodes having porosity above 85% and fibers of size 1-2 µm in diameter [16]. These properties are substantially different from those of commercially available carbon paper. To evaluate the model predictions, Liu et al [15] used

electrospinning to produce a fibrous electrode with the predicted optimum physical properties suggested by Kok et al [16] and tested it in an all-vanadium redox flow battery (VRFB). A performance comparison between this electrospun material and a commercial carbon paper (SGL25AA, widely used for VRFBs) showed that the electrospun electrode exhibited better performance in the activation region, and higher power density in comparison to the commercial carbon paper electrode [15]. Thus, electrospinning smaller fibers resulted in increased surface area, improved reaction rates and RFB power density. The present study focused on developing a proof-of-concept material to demonstrate the effect changing the electrospun fiber morphology from cylindrical to flat ribbons will have on RFB performance. The ribbon morphology should increase the surface-to-volume ratio of the material, increasing the reactive surface area per volume, while simultaneously improving the permeability. The material was successfully tested *in situ* in a flow-through cell, to demonstrate the feasibility of the structure in operation.

2. Materials and Methods

Polyacrylonitrile (PAN) was used as a precursor for fabricating electrodes because of its high theoretical carbon yield [15]. PAN has been widely used to electrospin carbon fibers, however, to the best of authors' knowledge, flat ribbons made of carbonized PAN have not been reported. Moreover, the change in electrospun fiber morphology from cylindrical to flat ribbon for various other polymers have mostly been achieved by changing electrospinning parameters, such as polymer concentration [17]–[20], applied voltage [19], ambient temperature [20], molecular weight [21], [22], etc. However, the technique proposed in the current study for making PAN ribbons is novel, relatively low effort, and more reliable compared to those mentioned in literature for polymers, such as nylon 11 [17], polystyrene [18], poly(ether imide) [18], gelatin [19], silk [20], polyvinylalcohol [21], and poly (ω-pentadecalactone) [22].

2.1. Materials

PAN (average MW 150,000), polystyrene (PS) (average MW 280,000), N,N-dimethylformamide (DMF) (99.8%) and chloroform (99.8%) were purchased from Sigma-Aldrich and used as received. The polymer solutions supplied to the shell and the core of the coaxial needle were prepared by dissolving PAN in DMF and PS in DMF, respectively, in ratios described in the next section. The solutions were stirred for 20 h without heating to prepare a homogeneous mixture.

2.2. Fabrication of ribbon-based electrode

The electrospun mat was fabricated using a custom-built coaxial electrospinning setup shown in Figure 1. The conditions for obtaining optimal electrodes were explored by preparing a range of possible combinations of shell solution (PAN/DMF) concentration of 9, 12 and 13.5 wt% and core solution (PS/DMF) concentration of 30, 33 and 35 wt%. This was done to determine the shell solution and core solution concentration combinations that produced ribbons most reliably and efficiently. The concentration of the spin dopant plays a crucial role in all electrospinning operations. A low concentration polymer solution leads to bead formation instead of uniform fibers; whereas, a high concentration makes electrospinning difficult because of high viscosity. As such, special attention was paid to finding the lower and upper concentration limits for both shell and core solutions. The flow rates for both shell and core solutions were maintained at 1.0 $mL \cdot h^{-1}$ and were decreased over time to ensure steady electrospinning [15], while maintaining a shell solution to core solution flow rate ratio of 1:1. A coaxial needle of shell size 11 ga and core size 14 ga was used to electrospin all samples and a distance of 9 cm was maintained between the needle and the collector. During electrospinning, a negative voltage of 15 kV was supplied to the collector drum, while the needle and all other

components were grounded [23]. After electrospinning, the fibrous mat was submerged in liquid chloroform for 24 h to extract PS from the core. After extraction was complete (24 h in all cases), the mat was removed from chloroform and dried at room temperature in a fume hood, confirmed by repeat weighing until the mass remained constant. This process resulted in a hollow core, which led to the collapse of the shell into PAN ribbons.

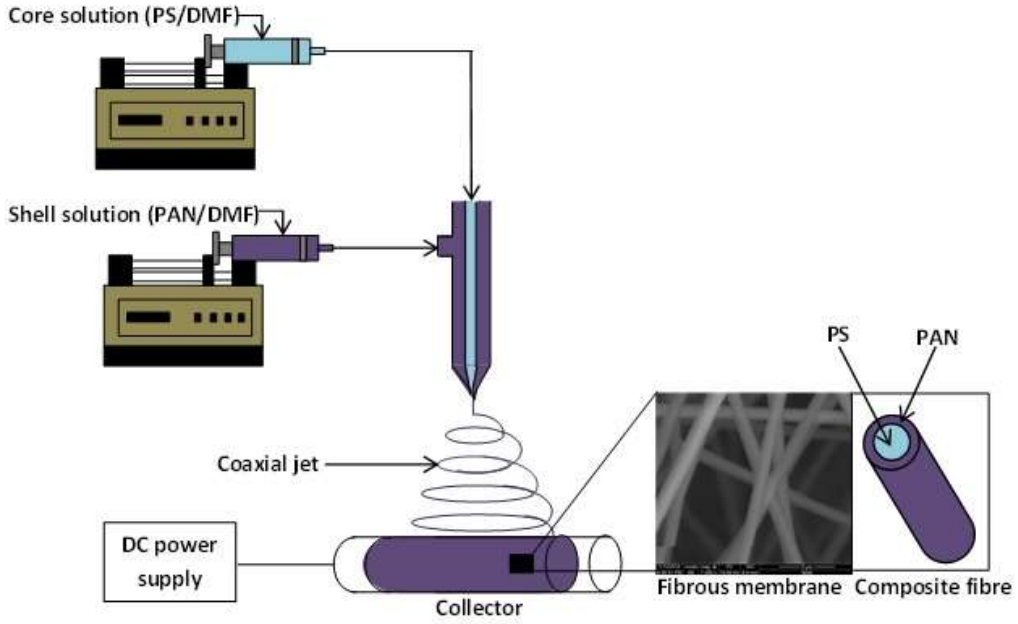

Figure 1: Coaxial electrospinning setup used for fabricating composite fibers.

2.3. Carbonization

After synthesis, the fibrous mat was carbonized in a MTI-GSL-1700X Alumina tube furnace using the standard procedure mentioned in literature [24]–[26]. Stabilization was carried out in the presence of air by heating the sample from room temperature to 250 °C and then maintaining it at 250 °C for 3 h. At 2 h and 45 min into the stabilization process, the gas was transitioned to pure nitrogen at a flow rate of 200 sccm. After the stabilization process was complete, the temperature was increased and maintained at the following temperatures: 850, 1050 and 1500 °C for 40 minutes each. The furnace was then cooled from 1500 °C to 250 °C, followed by air cooling to room temperature. A constant heating rate of 5 °C·min^{-1} was used throughout all the above procedures.

2.4. Characterization

2.4.1. Imaging and Analysis

The ribbon morphology, shape and size were observed with a scanning electron microscope (SEM, Quanta FEG 250). The SEM images were analysed in ImageJ software to determine fiber diameter and ribbon width. X-ray computed tomography was utilized to inspect the internal structure of the materials and to assess the thickness of the ribbons that was not visible in the SEMs. A nano-computed tomography (nano-CT) instrument (Zeiss Xradia Ultra 810, Carl Zeiss Inc., Pleasanton, CA) was used to acquire the X-ray images. The instrument contains a Cr anode source with an accelerating voltage of 35 kV, producing a quasi-monochromatic beam at the Cr-Kα emission line of 5.4 KeV. A Fresnel zone plate was employed as the objective element to produce a magnified image on a 1024 × 1024 pixel

detector. Images were acquired in large field-of-view mode with no binning resulting in a 63.1 µm voxel size. The sample was rotated through 180° with 1601 radiographs each collected with a 35 s exposure. The radiographs were reconstructed using proprietary software (XMReconstructor, Carl Zeiss Inc.) using a parallel beam reconstruction algorithm. The very high resolution combined with the low energy of the lab nano-CT system means the samples require careful preparation to ensure sufficient x-ray transmission. This study followed the best practices developed and presented in previous work on nano-CT of electrospun materials [27], [28].

2.4.2. Physical Properties

Electrode porosity was measured using the buoyancy method, which has been shown to work well for thin, highly porous media [15], [29]. Vapor sorption analysis was used to obtain the sample specific surface area [$m^2 \cdot g^{-1}$] using a DVS Resolution device from Surface Measurement Systems. Cyclohexane was used as the adsorbate, and BET theory was used to extract surface area from the isotherms. In-plane permeability was also measured using a technique developed for thin fibrous media [30] and employed for electrospun materials in several studies [15], [23]. Lastly, electrical conductivity was measured using the van der Pauw technique which has also been validated for thin fibrous electrode materials [31].

2.5. Flow Battery Validation

To examine the performance of the ribbon electrodes in a battery, they were tested in a vanadium-based RFB [32] (VRFB) and compared to a commercial carbon paper (Freudenberg H23) as a baseline. The VRFB cell geometry, start-up, chemistries, and polarization testing procedure are identical to our prior report [15]. However, in this study, two commercial electrodes were stacked for each side of the flow cell, whereas previously one was used per side. The flow was injected in a flow-through configuration [33] for both cases, to constrain the comparison to the improvements in the in-plane flow obtained by the proposed structure. Prior to the electrochemical measurements, the electrolyte, under humidified nitrogen sparge, flowed (10 $mL \cdot min^{-1}$) through the reactor at open circuit voltage for 50 min to promote electrode wetting.

3. Results and Discussion

Figure 2 shows a set of SEM images of the electrospun ribbons made from different concentration ratios, after being subjected to 24 h of PS extraction. The fibers spun using the lowest concentration of PAN and PS, i.e., 9 wt% PAN in the shell and 30 wt% PS in the core led to a high yield of ribbons after PS extraction for 24 h; whereas, the other combinations of PAN and PS concentrations resulted in a larger proportion of cylindrical fibers. This can be explained by the shell geometry as higher PAN concentration results in a thicker shell that hinders PS extraction and reduces the volume fraction of the core. However, using higher concentrations of PS increased the amount of PS in the fiber core therefore requiring a greater extraction time. Thus, the concentration combination of 9 wt% PAN/DMF in the shell and 30 wt% PS/DMF in the core was selected for a detailed study of ribbon properties, such as size and aspect ratio, porosity, surface area and ultimately battery performance.

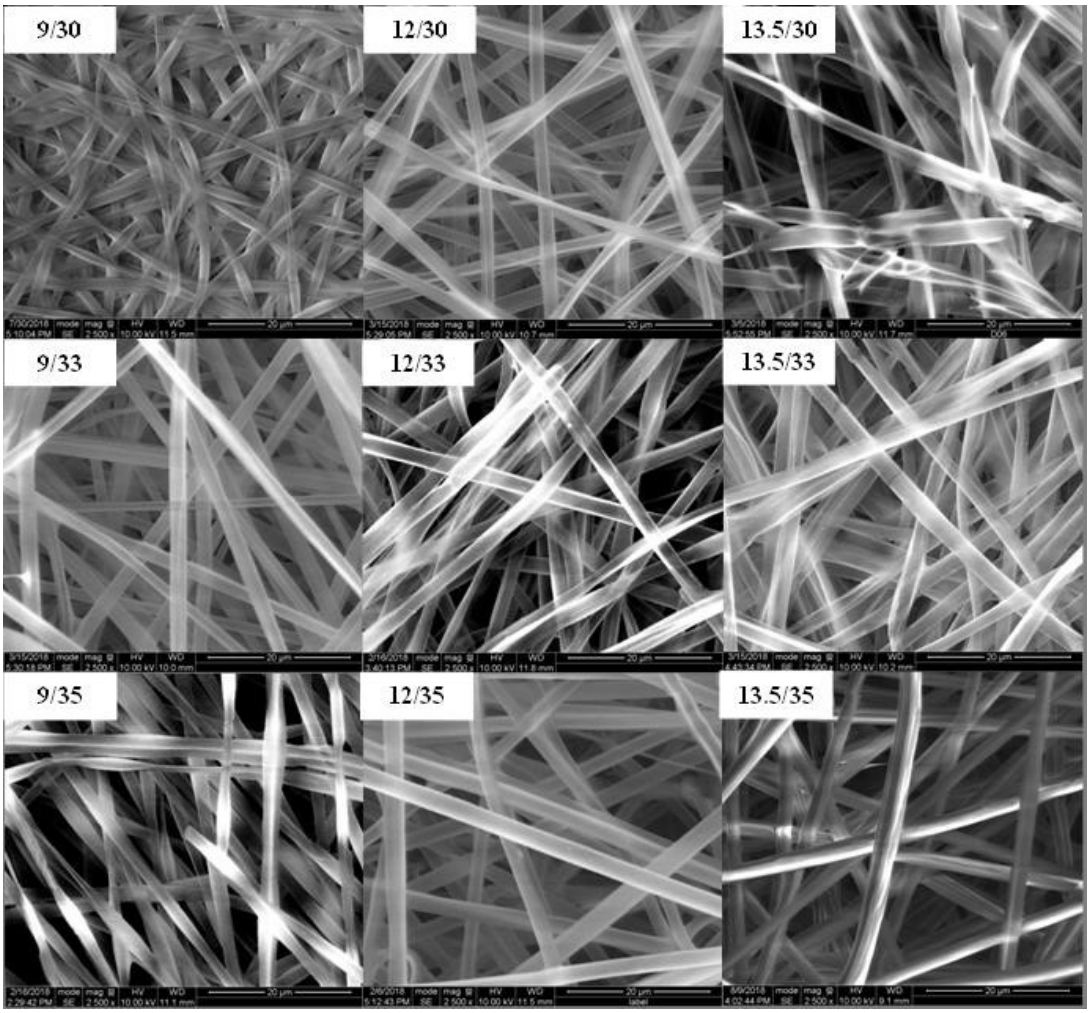

Figure 2: SEM images of fibers produced using varying shell and core solution concentrations (represented as shell/core solution wt%). Images are of materials after 24 hr extraction step. All images are taken at 2500× magnification. The scale bar is 20 µm.

Figure 3 shows an image of commercial Freudenberg H23 carbon paper and the coaxially electrospun fibers (shell: 9 wt% PAN/DMF and core: 30 wt% PS/DMF) prior to extraction of the PS core. It is evident from these images that the electrospinning technique produced significantly smaller fibers (diameter: 1.3 ± 0.1 µm) compared to the commercial Freudenberg H23 paper (diameter: 10.1 ± 0.3 µm) [34], [35]. After 24 h of PS extraction in chloroform, the electrospun composite cylindrical fibers shown in Figure 3B collapsed to form ribbons, as shown in Figure 4A. These ribbons were dried to remove chloroform and carbonized in the tube furnace to form carbon felt electrodes that comprised ribbon shaped fibers depicted in Figure 4B.

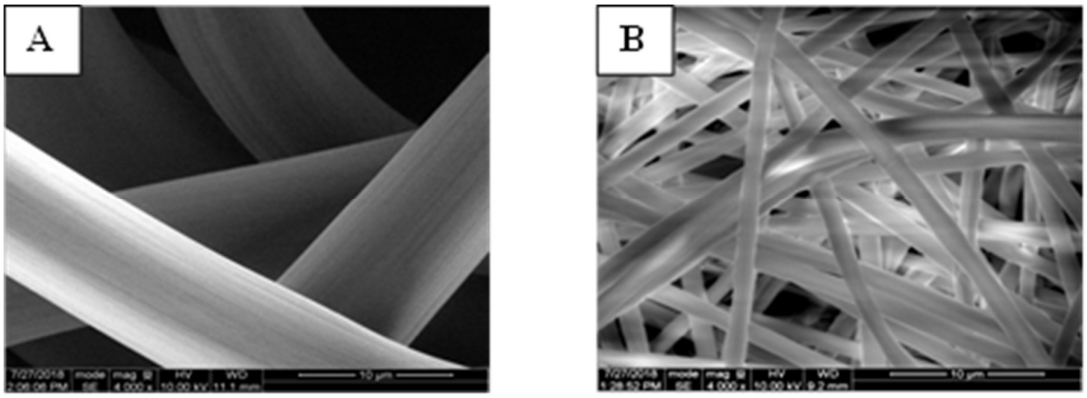

Figure 3: SEM images of (A) Freudenberg H23 and (B) coaxially electrospun composite cylindrical fibers made using 9 wt% PAN/DMF in the shell and 30 wt% PS/DMF in the core. Both images are at 4000× magnification and the scale bar is 10 µm.

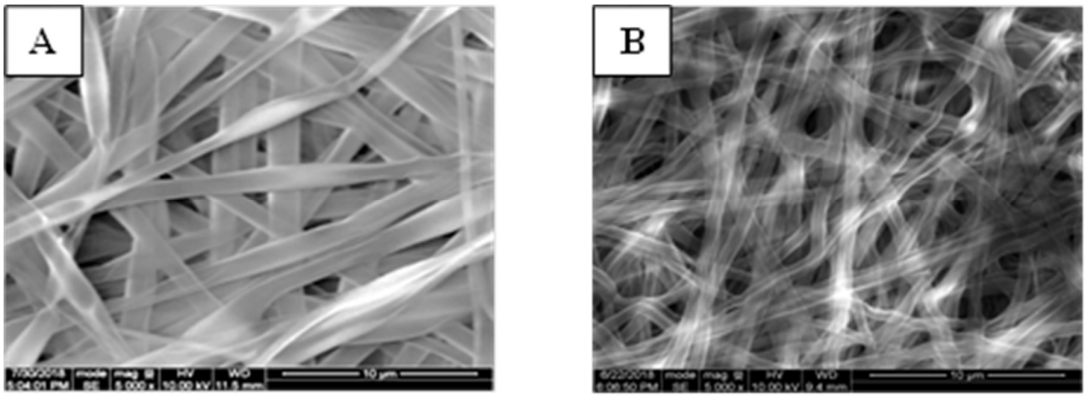

Figure 4: SEM images of (A) uncarbonized and (B) carbonized ribbons at 5000× magnification and 10 µm scale bar.

Due to mass loss during carbonization, the width of the ribbons was 1.5 µm before carbonization but 0.8 µm after carbonization. X-ray tomography was applied to study the internal structure of the carbonized ribbons, yielding the images shown in Figure 5. The thickness of the ribbons, which is difficult to determine from the 2D SEM images, was obtained from tomograms by performing a skeletonization of the solid phase to obtain the medial axis of the fibers. The medial axis was then used as a mask on the distance transform of the solid phase. The histogram of the surviving voxels had a peak at 214 nm meaning that the medial axis was within 214 nm from the nearest wall on average. Due to the ribbon-like geometry of the solid, this value represents half of the ribbon thickness, indicating that the ribbons were approximately twice as wide as they were thick (800 nm vs 430 nm), which agrees with a visual inspection of Figure 5.

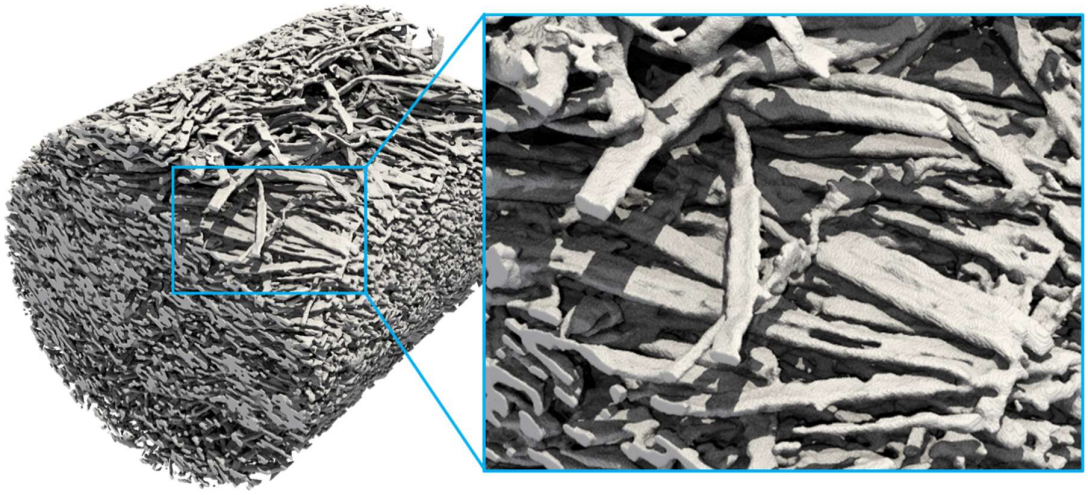

Figure 5: X-ray tomograms of the carbonized ribbons. The inset shows a closeup revealing the considerable width to thickness aspect ratio of the flat fibers

The porosity of the uncompressed ribbon electrode and Freudenberg H23 carbon paper were determined, with the ribbon electrode exhibiting a substantially higher porosity (92.6%) as compared to the Freudenberg H23 electrode (72.5%) [29], [34]. The properties of the ribbon electrode were also similar to the optimum properties determined by Kok et al [16]. Finally, it was confirmed that the ribbon-based carbon felt displayed an excellent permeability. Permeability values are difficult to compare directly due to differences in fiber size and porosity, so the Carman-Kozeny correlation is often used. In the present case however, the uniquely shaped ribbons meant that even this normalization is not suitable since the characteristic length of the ribbons is not a single value. Instead, the raw permeability values are plotted as a function of porosity in Figure 6. From this data it can be concluded that the permeability of the uncarbonized ribbons is higher than the commercial Freudenberg H23 carbon paper due to their substantially higher porosity. Had the samples been compared at the same porosity, the custom materials would have been orders of magnitude less permeable, but the benefit of using sub-micron fibers is that high surface area and high porosity can be achieved simultaneously. Carbonization of the ribbons resulted in a further increase in porosity due to loss of material, and this yielded an increase in permeability relative to the uncarbonized ribbons (electrospun mat after PS extraction and drying). The average electrical conductivity of the ribbon electrode in the in-plane direction was 1714 $S \cdot m^{-1}$, compared to 4120 $S \cdot m^{-1}$ for the Freudenberg H23 material. A carbonization temperature of 1500 °C was used in this work, so a higher temperature could be used to increase conductivity if necessary. However, the electrical conductivity of ribbon-based carbon paper electrode (1714 $S \cdot m^{-1}$) was found to be much higher than that of the electrolyte conductivity (<100 $S \cdot m^{-1}$) and was thus deemed sufficient.

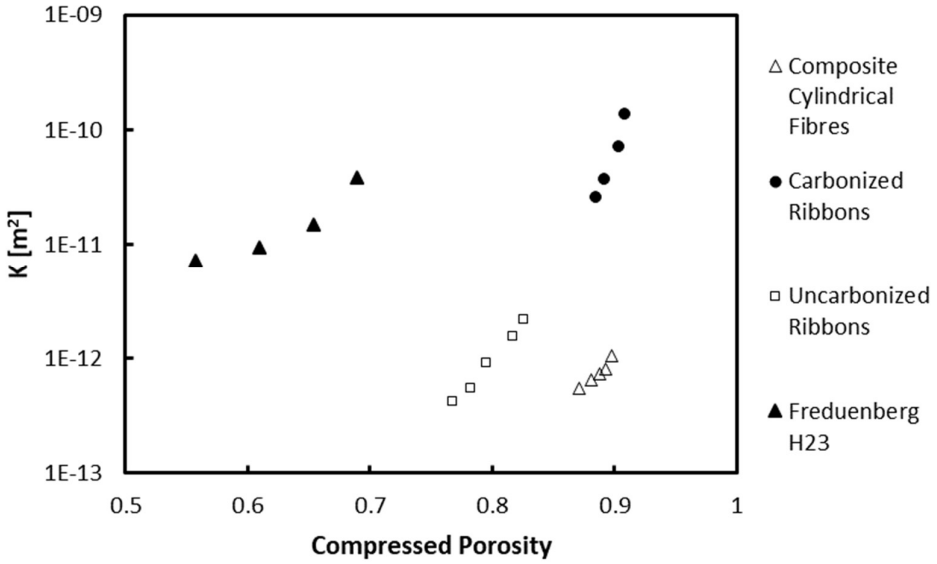

Figure 6: Permeability data for different stages of the ribbon materials plotted as a function of compressed porosity. For comparison Freudenberg H23 is plotted as well.

The specific surface area [$m^2 \cdot g^{-1}$] of electrodes were measured using DVS. However, the surface area per unit volume [$m^2 \cdot cm^{-3}$] was considered to be more important, because it defines the capacity of the electrode per unit volume and allows comparison of materials with different porosity and density. The volumetric surface area of Freudenberg H23 carbon paper, coaxially electrospun composite cylindrical fibers, uncarbonized ribbons and ribbon based electrodes were calculated to be 0.1088, 2.544, 4.431 and 4.057 $m^2 \cdot cm^{-3}$, respectively. As expected, electrospun fibers have more than 20× more surface area than commercial Freudenberg H23 paper per unit volume. Strikingly, changing the fiber morphology from cylinders to ribbons increased the surface area-to-volume ratio by an additional factor of 1.7. Since carbonization reduces mass and fiber width, the surface area to volume ratio of carbonized ribbons is slightly less than that of uncarbonized ribbons but greater than that of coaxially electrospun cylindrical fibers by a factor of 1.6. These results highlight the significant gains in volumetric surface area of electrodes that can be found by changing fiber morphology. In comparison to commercial Freudenberg H23 electrodes, the surface area per unit electrode volume of ribbons electrode was greater by a factor of 37.

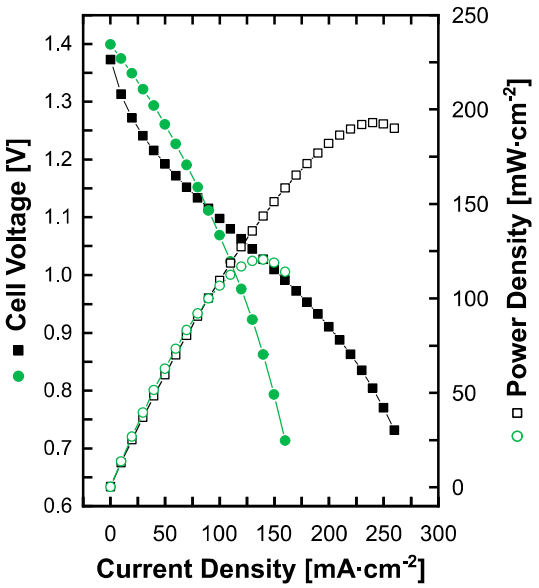

Figure 7: Comparison of the two electrodes in an all-vanadium redox flow battery. The polarization and power curves for the ribbon electrodes are shown in green, the Freudenberg H23 in black. All measurements were made at 50% SOC.

The ribbon and Freudenberg H23 electrodes were tested in a VRFB in order to illustrate the viability of the ribbon-based electrode, and compare relative performance. Figure 7 shows the polarization and power density curves of the electrodes, at 50% SOC. The cell was assembled with approximately 20% compression, which results in a reduction in the porosity of the electrode [36], consequently the porosity of the electrospun material was reduced to 90.8% and the Freudenberg material to 62.6%, assuming the solid volume does not change upon compression, thus the absolute permeability of the ribbon-based electrode remained substantially higher. From the polarization curves in Figure 7, it was observed that at lower current densities the VRFB cell voltage with the ribbon electrode was higher than that for the Freudenberg H23 electrode and shows almost no activation overpotential. This can be attributed to the higher volumetric surface area for the ribbon electrode, which enhances the electrode reaction rate that dominates voltage losses at low current densities. However, at current densities above ≈80 mA·cm^{-2}, the voltage drop for ribbon electrodes is rapid compared to the Freudenberg H23 material, signalling poor mass transfer or ion conduction in the former. This is because the ribbons appear to be too densely packed on the surfaces of the electrode (Figure 4), creating constrictions in through-plane transport within the electrolyte phase, thus adversely affecting mass and ion transfer at high current densities. Improving the pore structure to enhance the though-plane transport is therefore high priority for future work [37]. Recalling that the permeability of the ribbon electrodes was higher than the Freudenberg H23 electrode, it can also be expected that the parasitic pumping costs would be lower, further improving the system efficiency.

4. Conclusions

This study demonstrated a method for changing the fiber morphology in electrospun carbon paper materials from cylindrical to flat ribbons. A novel method was developed to prepare an electrospun mat of PAN ribbons based on coaxial electrospinning of a core-shell structure, followed by solvent extraction of the core. The surface area analysis shows that ribbons offer a $\sim 2x$ higher surface area-to-volume ratio than cylindrical fibers as well as $\sim 40x$ higher than commercial Freudenberg H23 carbon paper. These custom materials were shown to have a higher in-plane permeability than the commercial electrode despite their small fiber diameter. Ribbon electrodes ultimately exhibited

better performance in the activation region, and consequently higher power density than commercial materials at low current density when tested in a VRFB. This combined with the higher permeability suggests that such structures could both increase the electrochemical efficiency of the system as well as decrease the parasitic pumping costs. However, due to poor mass transfer in the ribbon electrode, significant voltage loss occurred at high current densities. Future work will focus on improving the through-plane mass transfer properties of ribbon electrode to improve high current density operation.

5. Conflicts of Interest

There are no conflicts to declare.

6. Acknowledgements

This work was supported by NSERC via the Discovery Grant program and the NSERC CREATE ME^2. The authors acknowledge the EPSRC and UCL for access to the nano CT instrument under grant EP/K005030/1, and P.R.S. acknowledges funding from the Royal Academy of Engineering under CiET1718/59. A.F.C., K.M.T., Y.M.C., and F.R.B. acknowledge funding from the Joint Center for Energy Storage Research that is an Energy Innovation Hub funded by the US Department of Energy (De-Ac02-06CH11357). K.M.T. recognizes additional funding from the US National Science Foundation Graduate Research Fellowship (1122374). Any opinion, findings, and conclusions or recommendations expressed in this material are those of the authors(s) and do not necessarily reflect the views of the National Science Foundation.

7. References

[1] H. Zheng, J. Li, X. Song, G. Liu, and V. S. Battaglia, "A comprehensive understanding of electrode thickness effects on the electrochemical performances of Li-ion battery cathodes," *Electrochimica Acta*, vol. 71, pp. 258–265, Jun. 2012, doi: 10.1016/j.electacta.2012.03.161.

[2] R. Zhao, J. Liu, and J. Gu, "The effects of electrode thickness on the electrochemical and thermal characteristics of lithium ion battery," *Applied Energy*, vol. 139, pp. 220–229, Feb. 2015, doi: 10.1016/j.apenergy.2014.11.051.

[3] B. R. Chalamala, T. Soundappan, G. R. Fisher, M. R. Anstey, V. V. Viswanathan, and M. L. Perry, "Redox flow batteries: An engineering perspective," *Proceedings of the IEEE*, vol. 102, no. 6, 2014, doi: 10.1109/JPROC.2014.2320317.

[4] E. Ali, H. Kwon, J. Choi, J. Lee, J. Kim, and H. Park, "A numerical study of electrode thickness and porosity effects in all vanadium redox flow batteries," *Journal of Energy Storage*, vol. 28, p. 101208, Apr. 2020, doi: 10.1016/j.est.2020.101208.

[5] M. R. Mohamed, S. M. Sharkh, and F. C. Walsh, "Redox flow batteries for hybrid electric vehicles: Progress and challenges," in *5th IEEE Vehicle Power and Propulsion Conference, VPPC '09*, 2009, pp. 551–557, doi: 10.1109/VPPC.2009.5289801.

[6] K. Amini, J. Gostick, and M. D. Pritzker, "Metal and Metal Oxide Electrocatalysts for Redox Flow Batteries," *Advanced Functional Materials*, vol. 30, no. 23, p. 1910564, 2020, doi: 10.1002/adfm.201910564.

[7] C. Busacca, O. D. Blasi, G. Giacoppo, N. Briguglio, V. Antonucci, and A. D. Blasi, "High performance electrospun nickel manganite on carbon nanofibers electrode for vanadium redox flow battery," *Electrochimica Acta*, vol. 355, p. 136755, Sep. 2020, doi: 10.1016/j.electacta.2020.136755.

[8] Y. Gao *et al.*, "Carbon sheet-decorated graphite felt electrode with high catalytic activity for vanadium redox flow batteries," *Carbon*, vol. 148, pp. 9–15, Jul. 2019, doi: 10.1016/j.carbon.2019.03.035.

[9] D. S. Aaron *et al.*, "Dramatic performance gains in vanadium redox flow batteries through modified cell architecture," *Journal of Power Sources*, vol. 206, pp. 450–453, May 2012, doi: 10.1016/j.jpowsour.2011.12.026.

[10] X. Ke, J. M. Prahl, I. J. D. Alexander, J. S. Wainright, T. A. Zawodzinski, and R. F. Savinell, "Rechargeable redox flow batteries: Flow fields, stacks and design considerations," *Chemical Society Reviews*, vol. 47, no. 23. Royal Society of Chemistry, pp. 8721–8743, Dec. 01, 2018, doi: 10.1039/c8cs00072g.

[11] X. L. Zhou, Y. K. Zeng, X. B. Zhu, L. Wei, and T. S. Zhao, "A high-performance dual-scale porous electrode for vanadium redox flow batteries," *Journal of Power Sources*, vol. 325, pp. 329–336, Sep. 2016, doi: 10.1016/j.jpowsour.2016.06.048.

[12] M. H. Moghim, R. Eqra, M. Babaiee, M. Zarei-Jelyani, and M. M. Loghavi, "Role of reduced graphene oxide as nano-electrocatalyst in carbon felt electrode of vanadium redox flow battery," *Journal of Electroanalytical Chemistry*, vol. 789, pp. 67–75, Mar. 2017, doi: 10.1016/j.jelechem.2017.02.031.

[13] J. Ryu, M. Park, and J. Cho, "Catalytic Effects of B/N-co-Doped Porous Carbon Incorporated with Ketjenblack Nanoparticles for All-Vanadium Redox Flow Batteries," *Journal of The Electrochemical Society*, vol. 163, no. 1, pp. A5144–A5149, 2016, doi: 10.1149/2.0191601jes.

[14] M. Z. Jelyani, S. Rashid-Nadimi, and S. Asghari, "Treated carbon felt as electrode material in vanadium redox flow batteries: a study of the use of carbon nanotubes as electrocatalyst," *Journal of Solid State Electrochemistry*, vol. 21, no. 1, pp. 69–79, Jan. 2017, doi: 10.1007/s10008-016-3336-y.

[15] S. Liu, M. Kok, Y. Kim, J. L. Barton, F. R. Brushett, and J. Gostick, "Evaluation of Electrospun Fibrous Mats Targeted for Use as Flow Battery Electrodes," *Journal of The Electrochemical Society*, vol. 164, no. 9, pp. A2038–A2048, 2017, doi: 10.1149/2.1301709jes.

[16] M. D. R. Kok, A. Khalifa, and J. T. Gostick, "Multiphysics Simulation of the Flow Battery Cathode: Cell Architecture and Electrode Optimization," *Journal of The Electrochemical Society*, vol. 163, no. 7, pp. A1408–A1419, May 2016, doi: 10.1149/2.1281607jes.

[17] M. Dhanalakshmi and J. P. Jog, "Preparation and characterization of electrospun fibers of Nylon 11," *Express Polymer Letters*, vol. 2, no. 8, pp. 540–545, Aug. 2008, doi: 10.3144/expresspolymlett.2008.65.

[18] S. Koombhongse, W. Liu, and D. H. Reneker, "Flat polymer ribbons and other shapes by electrospinning," *Journal of Polymer Science, Part B: Polymer Physics*, vol. 39, no. 21, pp. 2598–2606, Nov. 2001, doi: 10.1002/polb.10015.

[19] F. Topuz and T. Uyar, "Electrospinning of gelatin with tunable fiber morphology from round to flat/ribbon," *Materials Science and Engineering: C*, vol. 80, pp. 371–378, Nov. 2017, doi: 10.1016/j.msec.2017.06.001.

[20] N. Amiraliyan, M. Nouri, and M. H. Kish, "Effects of some electrospinning parameters on morphology of natural silk-based nanofibers," *Journal of Applied Polymer Science*, vol. 113, no. 1, pp. 226–234, Jul. 2009, doi: 10.1002/app.29808.

[21] A. Koski, K. Yim, and S. Shivkumar, "Effect of molecular weight on fibrous PVA produced by electrospinning," *Materials Letters*, vol. 58, no. 3–4, pp. 493–497, Jan. 2004, doi: 10.1016/S0167-577X(03)00532-9.

[22] E. R. Pavlova, I. E. Nifant'ev, M. E. Minyaev, D. V Bagrov, and D. V Klinov, "Mechanical properties and morphology of electrospun mats made of poly (ω-pentadecalactone)," p. 12013, 2019, doi: 10.1088/1742-6596/1310/1/012013.

[23] M. D. R. Kok and J. T. Gostick, "Transport properties of electrospun fibrous membranes with controlled anisotropy," *Journal of Membrane Science*, vol. 473, pp. 237–244, Jan. 2015, doi: 10.1016/j.memsci.2014.09.017.

[24] E. Fitzer, W. Frohs, and M. Heine, "Optimization of stabilization and carbonization treatment of PAN fibres and structural characterization of the resulting carbon fibres," *Carbon*, vol. 24, no. 4, pp. 387–395, Jan. 1986, doi: 10.1016/0008-6223(86)90257-5.

[25] M. S. A. Rahaman, A. F. Ismail, and A. Mustafa, "A review of heat treatment on polyacrylonitrile fiber," *Polymer Degradation and Stability*, vol. 92, no. 8. Elsevier, pp. 1421–1432, Aug. 01, 2007, doi: 10.1016/j.polymdegradstab.2007.03.023.

[26] N. Yusof and A. F. Ismail, “Post spinning and pyrolysis processes of polyacrylonitrile (PAN)-based carbon fiber and activated carbon fiber: A review,” *Journal of Analytical and Applied Pyrolysis*, vol. 93. Elsevier B.V., pp. 1–13, 2012, doi: 10.1016/j.jaap.2011.10.001.

[27] R. Jervis, M. D. R. Kok, J. Montagut, J. T. Gostick, D. J. L. Brett, and P. R. Shearing, “X-ray Nano Computed Tomography of Electrospun Fibrous Mats as Flow Battery Electrodes,” *Energy Technology*, vol. 6, no. 12, pp. 2488–2500, 2018, doi: 10.1002/ente.201800338.

[28] M. D. R. Kok, R. Jervis, D. Brett, P. R. Shearing, and J. T. Gostick, “Insights into the Effect of Structural Heterogeneity in Carbonized Electrospun Fibrous Mats for Flow Battery Electrodes by X-Ray Tomography,” *Small*, vol. 14, no. 9, p. 1703616, 2018, doi: 10.1002/smll.201703616.

[29] R. R. Rashapov, J. Unno, and J. T. Gostick, “Characterization of PEMFC Gas Diffusion Layer Porosity,” *Journal of The Electrochemical Society*, vol. 162, no. 6, pp. F603–F612, Mar. 2015, doi: 10.1149/2.0921506jes.

[30] J. T. Gostick, M. W. Fowler, M. D. Pritzker, M. A. Ioannidis, and L. M. Behra, “In-plane and through-plane gas permeability of carbon fiber electrode backing layers,” *Journal of Power Sources*, vol. 162, no. 1, pp. 228–238, Nov. 2006, doi: 10.1016/j.jpowsour.2006.06.096.

[31] D. R. P. Morris and J. T. Gostick, “Determination of the in-plane components of the electrical conductivity tensor in PEM fuel cell gas diffusion layers,” *Electrochimica Acta*, vol. 85, pp. 665–673, Dec. 2012, doi: 10.1016/j.electacta.2012.08.083.

[32] K. Lourenssen, J. Williams, F. Ahmadpour, R. Clemmer, and S. Tasnim, “Vanadium redox flow batteries: A comprehensive review,” *Journal of Energy Storage*, vol. 25, p. 100844, Oct. 2019, doi: 10.1016/j.est.2019.100844.

[33] J. D. Milshtein, K. M. Tenny, J. L. Barton, J. Drake, R. M. Darling, and F. R. Brushett, “Quantifying Mass Transfer Rates in Redox Flow Batteries,” *J. Electrochem. Soc.*, vol. 164, no. 11, p. E3265, May 2017, doi: 10.1149/2.0201711jes.

[34] A. Forner-Cuenca, E. E. Penn, A. M. Oliveira, and F. R. Brushett, “Exploring the Role of Electrode Microstructure on the Performance of Non-Aqueous Redox Flow Batteries,” *Journal of The Electrochemical Society*, vol. 166, no. 10, pp. A2230–A2241, Jun. 2019, doi: 10.1149/2.0611910jes.

[35] B. Chakrabarti *et al.*, “Charge/discharge and cycling performance of flexible carbon paper electrodes in a regenerative hydrogen/vanadium fuel cell,” *International Journal of Hydrogen Energy*, vol. 44, no. 57, pp. 30093–30107, Nov. 2019, doi: 10.1016/j.ijhydene.2019.09.151.

[36] L. D. Brown, T. P. Neville, R. Jervis, T. J. Mason, P. R. Shearing, and D. J. L. Brett, “The effect of felt compression on the performance and pressure drop of all-vanadium redox flow batteries,” *Journal of Energy Storage*, vol. 8, pp. 91–98, Nov. 2016, doi: 10.1016/j.est.2016.10.003.

[37] A. Gayon Lombardo, B. A. Simon, O. Taiwo, S. J. Neethling, and N. P. Brandon, “A pore network model of porous electrodes in electrochemical devices,” *Journal of Energy Storage*, vol. 24, p. 100736, Aug. 2019, doi: 10.1016/j.est.2019.04.010.